Volume 19, Number 3, 2026. pp. 325-335

Jordan Journal of Physics

ARTICLE

Laser-ablated Silver Nanoparticles in Deionized Water: Optical Characterization and Enhanced Antimicrobial Performance against Resistant Bacteria

Edrees E. Khadeer[a], **Aya M. Hazem**[a] and **Almashhadani, Mohammad Abdullah**[b]

[a] *Department of Physics, College of Science, University of Mosul, Mosul, Iraq.*
[b] *Department of Medical Physics, College of Science, University of Mosul, Mosul, Iraq.*

DOI: **https://doi.org/10.47011/19.3.4**
Received on: 14/04/2025; *Accepted on: 07/09/2025*

Abstract: This study investigates the synthesis of silver nanoparticles (AgNPs) using pulsed laser ablation in liquid (PLAL), focusing on the effect of laser pulse parameters on the optical, structural, and antimicrobial properties of produced AgNPs. The laser source was employed to ablate a high-purity silver target in deionized water, with pulse energies ranging from 400 to 1200 mJ. Characterization via UV spectroscopy revealed a surface plasmon resonance (SPR) peak at 320 nm, confirming AgNP formation, with absorption intensity and nanoparticle concentration increasing with higher pulse energy. Scanning electron microscopy (SEM) demonstrated spherical AgNPs (39.53–52.31 nm) with uniform size distribution, while X-ray diffraction (XRD) confirmed a face-centered cubic (FCC) crystal structure with a calculated lattice parameter of 4.08 Å, in excellent agreement with bulk silver. The antimicrobial efficacy of AgNPs was evaluated against multidrug-resistant Gram-negative (*Pseudomonas aeruginosa, Escherichia coli, Klebsiella pneumoniae*) and Gram-positive (*Staphylococcus aureus*) bacteria. The results showed dose-dependent inhibition, with maximal zones of inhibition (15–18 mm) at 1200 mJ, attributed to reactive oxygen species (ROS) generation and membrane disruption. Gram-negative bacteria exhibited higher sensitivity because of their thinner peptidoglycan layer. This work highlights the potential of laser-ablated AgNPs as a tunable and chemical-free alternative to combat antibiotic-resistant pathogens, with applications in nanomedicine and antimicrobial therapies.

Keywords: Silver nanoparticles (AgNPs), Pulsed laser ablation in liquid (PLAL), Antibacterial activity, UV-spectroscopy, Surface Plasmon Resonance (SPR), Nanoparticle synthesis, Antimicrobial Resistance (AMR), SEM & XRD characterization.

1. Introduction

Precious metals have captivated human civilization since ancient times. Among these, gold (Au), silver (Ag), platinum (Pt), and palladium (Pd) have served diverse roles throughout history - from functional applications in tools and ornaments to serving as monetary standards in early economies, particularly through gold and silver coinage. Silver, classified as a transition metal alongside copper and gold, possesses distinctive characteristics including its malleable nature, bright white luster, and excellent conductivity. In recent decades, silver nanoparticles (AgNPs) have gained significant attention across multiple scientific and industrial domains. Their exceptional physicochemical properties have led to widespread applications in medicine, healthcare technologies, food processing, and commercial products. Research has demonstrated their effectiveness as antimicrobial agents, with additional applications in orthopaedic implants, controlled drug delivery

Corresponding Author: Edrees E. Khadeer **Email**: dr.adrees@uomosul.edu.iq

systems, diagnostic imaging, and even as adjuvants in cancer therapy where they potentiate the cytotoxic effects of anticancer drugs [1]. Silver nanoparticles (AgNPs) rank among the most studied nanomaterials due to their exceptional properties and versatile applications. Their unique characteristics have generated significant scientific interest across multiple disciplines, including optoelectronics [2], chemical and biological sensing [3, 4], surface-enhanced Raman spectroscopy (SERS) [5, 6], and catalytic applications [7–9], as well as numerous other specialized fields [10–12]. Beyond these advanced technological applications, AgNPs demonstrate remarkable utility in practical scenarios. They serve as effective components in colloidal nano-dispersions, water treatment and disinfection systems [12, 13], thin-film dopants [14], and corrosion-resistant coatings [15]. This broad applicability has driven sustained research into developing controlled synthesis methods that precisely regulate nanoparticle characteristics, including size distribution, morphological uniformity, dispersion stability, and shape specificity. To achieve these objectives, researchers have developed numerous synthesis strategies: chemical reduction [16], biomechanochemical processing [17], electrochemical synthesis [18], photochemical approaches [19, 20], microwave-assisted synthesis [21], hydrothermal methods, pulsed laser ablation [22], sol-gel techniques [23], sonochemical synthesis [16, 24], and green synthesis routes [25, 26]. Each method offers distinct advantages in tailoring the physical and chemical properties of AgNPs for specific applications. The continued refinement of these techniques remains crucial for advancing nanomaterial-based technologies across scientific and industrial domains. A highly effective and innovative technique for generating metallic nanoparticles is laser ablation in liquid (LAL), where a bulk material is irradiated with a laser while submerged in a solution. This method stands out for its simplicity, adaptability, and ability to produce uncontaminated nanoparticles without requiring additional chemical reagents [27–34]. The efficiency of ablation and the properties of the resulting silver nanoparticles depend on several critical parameters: laser parameters (wavelength, power, and exposure time), choice of liquid medium, and use of stabilizing agents (surfactants) [35, 36]. To improve pulsed laser ablation in liquid (PLAL), researchers employ strategies such as implementing a continuous liquid flow system, reducing liquid-layer thickness, and conducting ablation in aqueous environments. However, water can sometimes degrade nanoparticle quality by promoting oxidation. In such cases, low-viscosity organic solvents serve as superior alternatives [37]. Additional studies have examined how different solvents influence the optical properties of ultrafine nanoparticles synthesized via this method [38]. Nanoparticles have garnered significant attention in scientific research because their exceptional, tunable properties differ markedly from those of their bulk counterparts, making them invaluable for advanced technological applications. While the PLAL technique for AgNP synthesis is well-established, many studies primarily focus on optimizing parameters for morphological control (size, shape) and basic optical characterization [e.g., 27, 39]. However, a significant research gap exists in systematically correlating these laser parameters (especially across a wide energy range: 400–1200 mJ) directly to the *functional antimicrobial efficacy* of the resulting nanoparticles, particularly against contemporary, clinically relevant multidrug-resistant (MDR) bacterial strains. Furthermore, comparative studies on the differential response of Gram-positive and Gram-negative MDR pathogens to laser-ablated AgNPs of defined sizes are limited. This work aims to bridge this gap by providing a comprehensive analysis from synthesis to application, explicitly linking laser energy to structural properties and, crucially, to enhanced antibacterial performance against a panel of resistant bacteria. This study focuses on synthesizing silver nanoparticles (AgNPs) through pulsed laser ablation in deionized water. The primary objective is to investigate how varying laser pulse energy influences key characteristics of the nanoparticles, including optical properties, structural features, morphology, and biological activity.

2. Experimental Work

2.1. Synthesis and Characterization of Silver Nanoparticles (AgNPs)

Silver nanoparticles (AgNPs) were synthesized using the pulsed laser ablation in Liquid (PLAL) technique. A high-purity silver disc (99.99%, 20 mm diameter × 2 mm

thickness) served as the ablation target. Prior to ablation, the target was ultrasonically cleaned in acetone for 5 minutes to remove surface contaminants, rinsed thoroughly with distilled water, and air-dried. The cleaned target was immersed in 7 mL of ultra-pure deionized water within a quartz beaker. A Q-switched Nd:YAG laser system (Table 1) operating at a wavelength of 1064 nm with a pulse duration of 10 ns was used as the ablation source. The laser beam was focused onto the surface of the silver target, which was positioned 65 mm from the laser source. To ensure uniform ablation and prevent pit formation, the target was continuously rotated at 10 rpm using an electric motor. The ablation process was carried out at varying pulse energies (400, 600, 800, 1000, and 1200 mJ) with a fixed 800 pulses per sample. The successful formation of AgNPs was indicated by a visual color change of the solution to light orange or gray. The experimental setup is illustrated in Fig. 1.

TABLE 1. Characteristics of the pulsed laser used.

Parameters	Value
Laser Type	*Q-switched Nd:YAG*
Laser Output Energy	*400, 600, 800, 1000, 1200 mJ*
Frequency	*2 Hz*
Wavelength	*1064 nm*
Laser Pulses	*800*
Pulse Duration	*10 ns*
Transverse Mode	*TEM00*

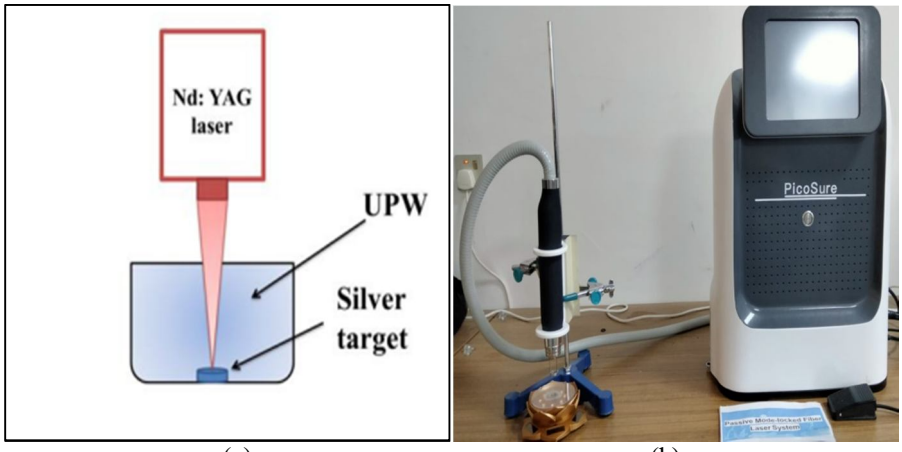

(a) (b)

FIG. 1. (a) Schematic [39] and (b) photographic image of the PLAL setup.

The synthesized colloidal AgNPs were characterized using the following techniques to determine their optical properties, morphology, size distribution, and crystal structure:

Ultraviolet-Visible (UV-Vis) Spectroscopy

The optical absorption spectra of the AgNP colloids were recorded immediately after synthesis using a Shimadzu UV-2550 UV-Vis spectrophotometer in the wavelength range of 300 to 1000 nm. Quartz cuvettes with a 1-cm path length were used, with deionized water as a blank reference. The spectra were analyzed to identify the surface plasmon resonance (SPR) peak and assess nanoparticle stability and concentration.

Field Emission Scanning Electron Microscopy (FESEM):

The morphological features and size distribution of the AgNPs were examined using a scanning electron microscope (Zeiss Sigma VP). A drop of the colloidal suspension was placed on a clean aluminum stub and allowed to dry at room temperature under ambient conditions to prepare the sample for imaging. The FESEM analysis was performed at an accelerating voltage of 20 kV.

X-Ray Diffraction (XRD):

The crystalline structure and phase composition of the laser-ablated AgNPs were determined by X-ray diffraction. The colloidal

suspension was drop-cast onto a glass slide and dried to form a thin film for analysis. XRD patterns were acquired using an X-ray diffractometer (Bruker D8 Advance) with Cu Kα radiation (λ = 1.5406 Å) operating at 40 kV and 40 mA. The data were collected over a 2θ range of 10° to 90° with a step size of ~0.1° and a scan speed of 8° per minute.

2.2. Antimicrobial Effects of Silver Nanoparticles on Resistant Bacteria

In this study, four bacterial isolates, *Staphylococcus aureus* (Gram-positive), *Pseudomonas aeruginosa*, *Klebsiella pneumoniae*, and *Escherichia coli* (Gram-negative), were obtained from the Department of Biology at the University of Mosul, Iraq. Initial identification was based on morphological characteristics, followed by confirmation using the Vitek 2 system, which also provided their antibiotic susceptibility profiles. To assess the antimicrobial efficacy of silver nanoparticles (AgNPs), the well diffusion method was employed against multidrug-resistant strains. Bacterial suspensions were adjusted to approximately 1.5×10^8 cells/mL (McFarland Standard), and 1.5 mL of each suspension was spread onto Mueller-Hinton agar plates. After 15 minutes, 6-mm wells were created, and varying concentrations of AgNPs (400, 600, 800, 1000, and 1200 mJ) were added. The plates were incubated at 37 °C for 24 hours, alongside control plates. Inhibition zone diameters (in mm) were measured to assess antimicrobial activity, with larger zones indicating higher efficacy [40]. Antimicrobial resistance (AMR) remains a pressing global issue, with regional variations necessitating alternative treatments such as nanotechnology-based solutions. Kirby-Bauer antibiotic susceptibility testing (Fig. 2, Table 2) showed that all tested strains exhibited complete resistance to ampicillin (25 µg) and sulfamethoxazole-trimethoprim (25 µg), underscoring the urgent need for novel antimicrobial agents.

TABLE 2. Antibiotic Susceptibility Test Results Using the Kirby-Bauer Method.

Bacteria Types	Inhibition zone /mm			
	Control	Levofloxacin (5 µg)	Ampicillin (25 µg)	Sulfamethoxazole & Trimethoprim (25 µg)
P. aeruginosa	0 mm	15 mm	R	R
K. pneumoniae	0 mm	13 mm	R	R
E. coli	0 mm	14 mm	R	R
S. aureus	0 mm	10 mm	R	R

R: Resistant.

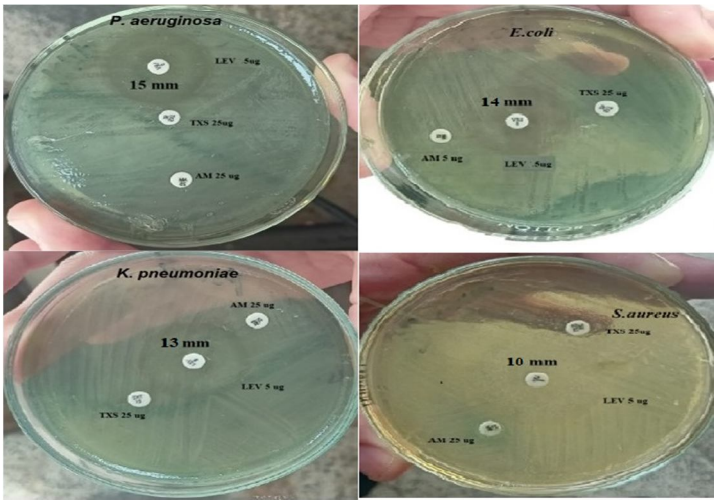

FIG. 2. Disk susceptibility testing for antibiotics using the Kirby-Bauer method.

The findings show widespread antibiotic resistance, with all tested bacterial strains completely resistant to ampicillin and sulfamethoxazole-trimethoprim; even levofloxacin (5 µg) showed reduced efficacy due to emerging resistance, severely limiting treatment options. This alarming trend stems from the overprescription and misuse of antibiotics in both clinical and agricultural settings, combined with the rapid horizontal

transfer of resistance genes among bacterial populations, creating a perfect storm for the emergence of untreatable infections. To address this critical public health threat, the implementation of rigorous antibiotic stewardship programs that mandate culture-guided prescriptions is essential, along with public education campaigns to promote responsible antibiotic use, while simultaneously accelerating research into alternative antimicrobial agents like silver nanoparticles to combat these increasingly resistant pathogens [41, 42].

3. Result and Discussion

UV-visible spectroscopy was employed to analyze the optical absorption profiles of the synthesized nanoparticles. A primary visual confirmation of successful nanoparticle formation was observed through distinct colorimetric changes in the aqueous solution, as illustrated in Fig. 3. The solution exhibited a progressive color transition to a characteristic greenish-gray hue, directly correlating with increasing laser energy levels, which served as a qualitative indicator of nanoparticle formation and size-dependent plasmonic effects.

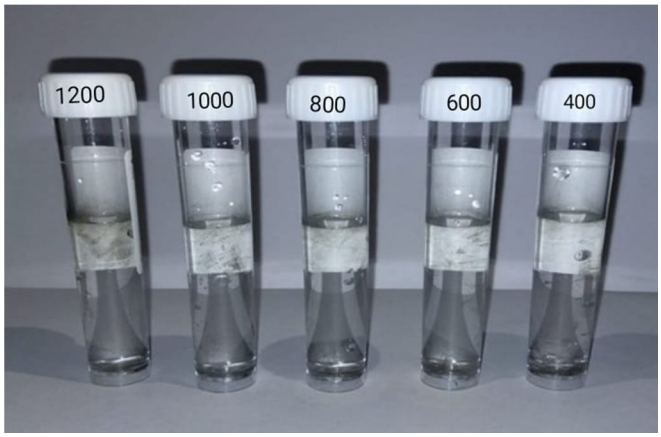

FIG. 3. AgNPs colloidal solutions produced by laser ablation at various laser energies (400–1200 mJ).

The SEM micrographs in Fig. 4 depict the morphology of Ag nanoparticles synthesized at a laser energy of 800 mJ. The images reveal spherical or quasi-spherical silver nanoparticles (AgNPs) with a narrow size distribution (39.53–52.31 nm) and high colloidal stability. This uniformity in shape and size suggests controlled crystallization and self-assembly during pulsed laser ablation in liquid (PLAL). The high laser energy facilitates rapid atomization of silver, leading to the formation of small, well-dispersed nanoparticles. Moreover, the process yields pure AgNPs with minimal contamination, enhancing their stability in solution. These observations are consistent with prior studies, e.g., Munaf et al. [43], who reported that PLAL-synthesized nanoparticles exhibit spherical morphology, small dimensions, high purity, and prolonged stability.

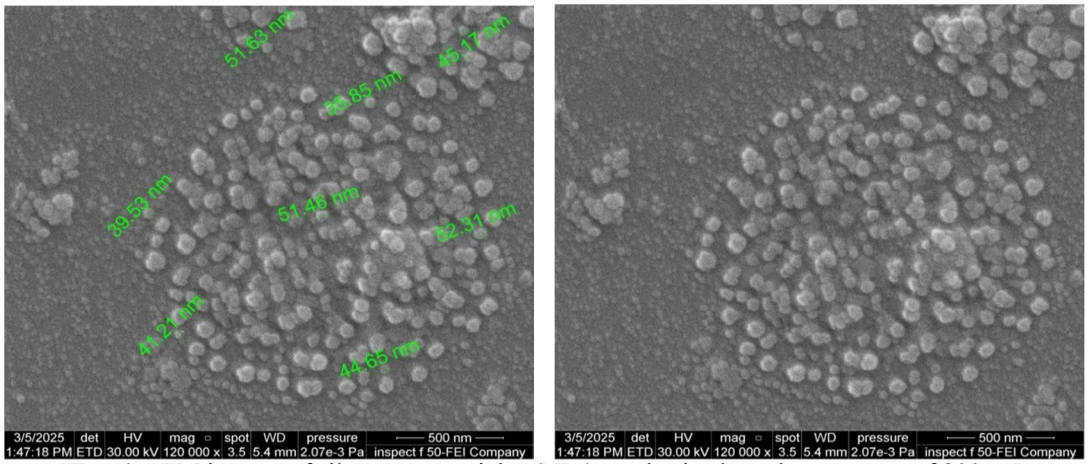

FIG. 4. SEM images of silver nanoparticles (NPs) synthesized at a laser energy of 800 mJ.

The XRD pattern of the synthesized silver nanoparticles (AgNPs) (Fig. 5) displays distinct diffraction peaks at 32.18°, 50.4°, and 74.1°, indexed to the (111), (200), and (220) crystallographic planes, respectively, of the face-centered cubic (FCC) structure of Ag NPs, which is the most stable crystalline phase for silver. Additionally, faint and broadened peaks appear at 29.5° and 62.8°, corresponding to the (110) and (211) planes. The broadening and low intensity of these peaks suggest ultrafine nanoparticles with a relatively low concentration in the sample. This effect may arise from factors such as prolonged storage between synthesis and XRD characterization, which can influence particle aggregation or oxidation. The observed peak broadening aligns with the Scherrer principle, where smaller crystallite sizes result in wider diffraction peaks due to reduced coherent scattering domains. These findings are in agreement with previous research [44], which reported similar XRD patterns for small-sized, low-concentration Ag NPs produced under comparable conditions.

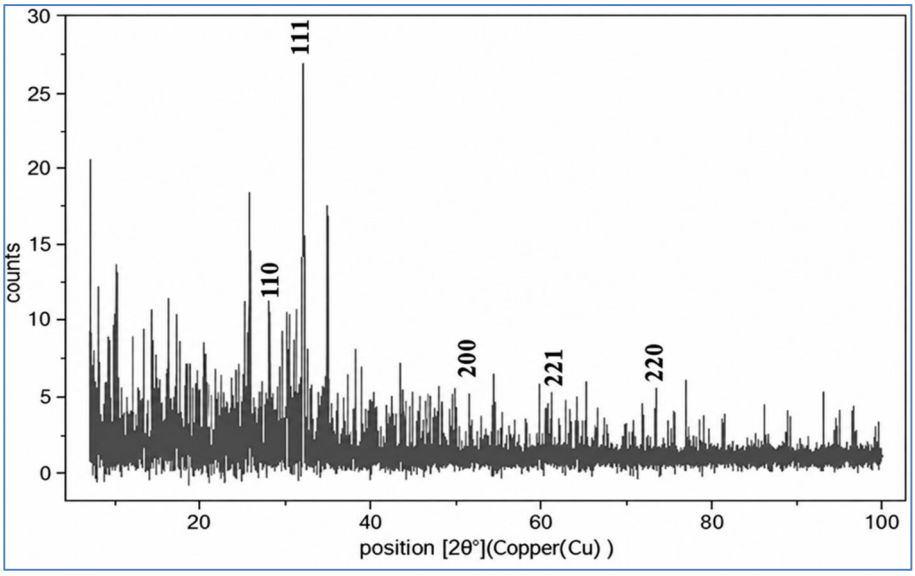

FIG. 5. X-ray diffraction (XRD) pattern of silver nanoparticles (NPs).

Using Bragg's law ($n\lambda = 2d \sin\theta$) and the relationship between the interplanar spacing (d) and the lattice parameter for a face-centered cubic (FCC) structure ($d_{hkl} = a / \sqrt{(h^2 + k^2 + l^2)}$), the lattice parameter a of the synthesized silver nanoparticles was determined from the (111) diffraction peak. The calculated value of approximately 4.08 Å is in excellent agreement with the standard lattice parameter for pure silver (4.086 Å, JCPDS card no. 04-0783), confirming the successful synthesis of phase-pure silver nanoparticles with an FCC crystal structure via the PLAL process. The minor deviation observed falls within the expected margin of error for XRD analysis and may be attributed to factors such as nanoscale strain or instrumental broadening [37].

UV-Vis spectroscopic characterization (Fig. 6) verified the successful formation of silver nanoparticles through pulsed laser ablation. Spectral analysis across the 320–1000 nm range revealed a characteristic surface plasmon resonance (SPR) band centered at 320 nm, providing definitive evidence of AgNP formation. This distinctive absorption feature results from coherent oscillations of surface electrons when excited by incident photons, a hallmark optical property of noble metal nanoparticles. The spectral profile exhibited strong absorption between 320–400 nm, matching the expected plasmonic response for colloidal silver nanostructures. The appearance of multiple overlapping peaks in this region suggests a polydisperse size distribution, with higher laser energies resulting in broader size variations. This energy-dependent size modulation was confirmed by observed changes in absorption characteristics. Notably, the optical absorption behavior demonstrated clear size dependence, with smaller nanoparticles exhibiting attenuated absorption due to their limited electron density and surface area, while larger particles showed enhanced absorption

from increased electron-photon interactions. These size-optical property correlations arise from quantum confinement effects governing the plasmonic responses of nanoscale silver systems, as documented in the literature [43].

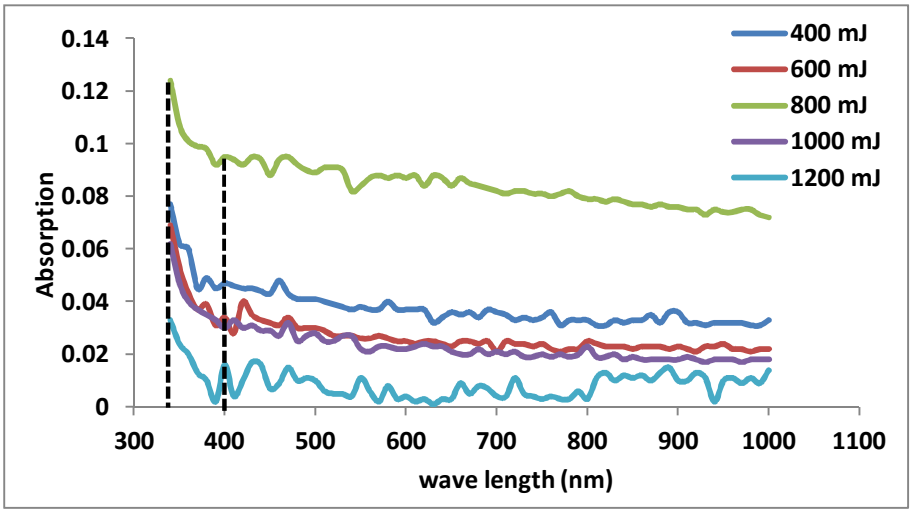

FIG. 6. UV-Vis spectra of silver nanoparticle colloidal solutions.

The antimicrobial efficacy of silver nanoparticles (AgNPs) synthesized at varying laser energies was evaluated against both Gram-positive and Gram-negative bacterial strains, as presented in Table 3. The measured inhibition zone diameters revealed a direct correlation between increasing laser energy and enhanced antibacterial activity, with Gram-negative bacteria generally exhibiting greater susceptibility than Gram-positive strains. The different responses can be attributed to variations in cell wall composition between bacterial types, where the thinner peptidoglycan layer of Gram-negative organisms facilitates nanoparticle penetration. The negative control showed no inhibitory effects, confirming that the observed antimicrobial activity was solely due to the AgNPs. These results demonstrate that laser energy parameters during synthesis can be optimized to produce AgNPs with tailored antibacterial properties for specific biomedical applications [45].

TABLE 3. Antibacterial activity of silver nanoparticles.

Bacteria types	negative control	AgNPs laser energy (mJ)				
		400 mJ	600 mJ	800 mJ	1000 mJ	1200mJ
		Inhibition zone (mm)				
P. aeruginosa	0	0	8	10	12	15
K. pneumoniae	0	0	10	12	13	18
E. coli	0	0	11	13	16	17
S. aureus	0	0	8	10	13	14

At an energy level of 400 mJ, no inhibition zones were observed in any of the tested bacterial species, indicating that this energy was insufficient to trigger the antibacterial properties of silver nanoparticles (AgNPs). The absence of inhibition suggests that 400 mJ falls below the minimum threshold required to activate AgNPs, meaning this energy level did not initiate significant antibacterial activity, such as silver ion release or reactive oxygen species (ROS) generation [46]. In contrast, at 600 mJ, measurable antibacterial activity was observed (Figs. 7 and 8). Among the tested bacteria, *E. coli* displayed the highest sensitivity, forming an 11 mm inhibition zone, while *P. aeruginosa* and *S. aureus* showed lower responsiveness, each with 8 mm zones. This confirms that 600 mJ exceeds the activation threshold for AgNPs, enabling detectable bacterial inhibition. Two primary mechanisms may explain this phenomenon [47, 48]:

1. Reactive oxygen species (ROS) production: At elevated energy levels, silver nanoparticles (AgNPs) exhibit enhanced generation of reactive oxygen species (ROS). These ROS

induce oxidative stress, damaging bacterial cell membranes, proteins, and DNA, ultimately leading to cell death.

2. Improved dispersion and bacterial interaction: Increased laser energy may also improve the dispersion and mobility of AgNPs, facilitating greater interaction with bacterial cells. This enhanced contact allows for more efficient delivery of antibacterial effects, such as silver ion release and membrane disruption.

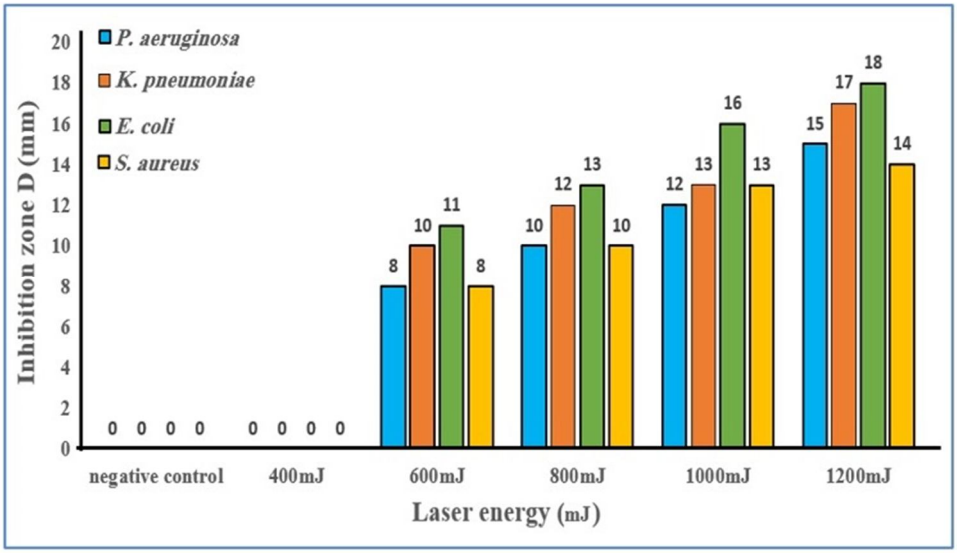

FIG. 7. Impact of varying laser energy (mJ) of the AgNPs on the tested bacteria.

When the laser energy was increased to 800 mJ, the inhibition zones expanded further. *E. coli* and *K. pneumoniae* remained the most sensitive species, exhibiting inhibition zones of 13 mm and 12 mm, respectively. In contrast, *P. aeruginosa* and *S. aureus* displayed smaller but equivalent zones of 10 mm. At 1000 mJ, *E. coli* demonstrated the strongest response, forming a 16 mm inhibition zone, while *P. aeruginosa* showed the least increase among the tested species, reaching only 12 mm. The highest energy level tested (1200 mJ) revealed distinct differences in bacterial susceptibility; *K. pneumoniae* exhibited the largest inhibition zone (18 mm), surpassing even *E. coli* (17 mm). This high sensitivity may be attributed to its thin peptidoglycan layer and outer membrane, which facilitate AgNP penetration and disruption of cellular processes [49]. Conversely, *S. aureus* displayed the lowest sensitivity, with only a 14 mm zone, likely due to its thick peptidoglycan cell wall, which hinders AgNP infiltration and contributes to its relative resistance [50].

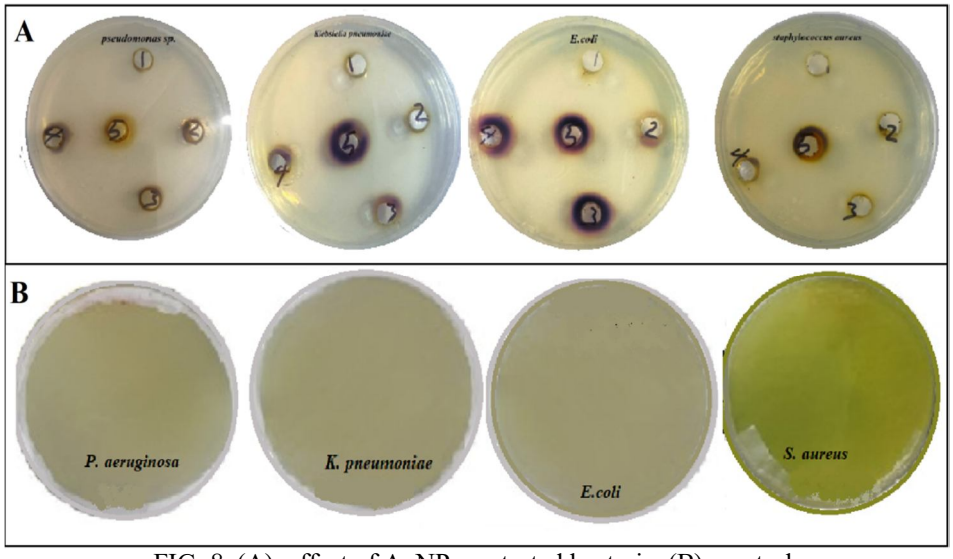

FIG. 8. (A): effect of AgNPs on tested bacteria, (B): control.

4. Conclusion

This study successfully synthesized silver nanoparticles (AgNPs) via pulsed laser ablation in liquid (PLAL), characterizing their optical properties and evaluating their antimicrobial effects against multidrug-resistant bacteria. The principal outcomes are outlined below:

- Spherical AgNPs with uniform size distribution (39.53–52.31 nm) were produced using a Q-switched Nd:YAG laser (532 nm, 10 ns pulse duration).
- XRD analysis verified a face-centered cubic (FCC) crystal structure, while UV spectroscopy detected a sharp surface plasmon resonance (SPR) peak at 320 nm, confirming successful nanoparticle formation.
- Increased laser energy (400–1200 mJ) enhanced absorption intensity, indicating higher nanoparticle yield and colloidal stability.
- The AgNPs demonstrated dose-dependent antibacterial effects, with the largest inhibition zones (15–18 mm) observed at the highest laser energy (1200 mJ).
- Gram-negative bacteria (*Pseudomonas aeruginosa*, *Escherichia coli*, *Klebsiella pneumoniae*) exhibited greater susceptibility than the Gram-positive *Staphylococcus aureus*, likely due to structural differences in their cell walls (thinner peptidoglycan layer in Gram-negative species).
- The proposed antimicrobial mechanism involved reactive oxygen species (ROS) production and cell membrane disruption, suggesting AgNPs as a promising alternative to traditional antibiotics.

Acknowledgment

Grateful acknowledgment is made to the Faculty of Science, Physics Department, for providing essential research facilities and academic support crucial for this study's completion. The department's scientific resources and expert guidance significantly contributed to this work's success.

Reference

[1] Chernousova, S. and Epple, M., Angew. Chem. Int. Ed., 52 (6) (2013) 1636.

[2] Hu, X. and Chan C.T., Applied Physics Letters, 85 (9) (2004) 1520.

[3] Alshehri, A.H., Jakubowska, M., Młożniak, A., Horaczek, M., Rudka, D., Free, Ch., and Carey, J.D., Applied Materials & Interfaces, 4 (12) (2012) 7007.

[4] Cobley, C.M., Skrabalak, S.E., Campbell, D.J., and Xia, Y., Plasmonics, 4 (2) (2009) 171.

[5] Nguyen, N.D., Nguyen, T.V., Chu, A.D., Tran, H.V., Tran, L.T., and Huynh, Ch.D., Arabian Journal of Chemistry, 11 (7) (2017) 1134.

[6] Li, Z., Wang, M., Jiao, Y., Liu, A., Wang, Sh., Zhang, Ch., Yang, Ch., Xu, Y., Li, Ch., and Man, B., Sensors and Actuators B: Chemical, 55 (2018) 374.

[7] Tao, L., Lou, Y., Zhao, Y., Hao, M., Yang, Y., Xiao, Y., Tsang, Y.H., and Li, J., Journal of Materials Science, 53 (1) (2018) 573.

[8] Ajitha, B., Kumar Reddy, Y.A., Jeon, H.-J., and Ahn, W.Ch., Advanced Powder Technology, 29 (1) (2018) 86.

[9] Young, J., Cheng, K., Young, Y., Chen, X., Chen, Y., Chang, T., Yen, H., and Chen, Ch., Carbohydrate Research, 457 (2018) 14.

[10] Asharani, I.V., Thirumalai, D., and Sivakumar, A., IOP Conference Series: Materials Science and Engineering, 263 (2017) 1.

[11] Franci, G., Falanga, A., Galdiero, S., Palomba, L., Rai, M., Morelli, G., and Galdiero, M., Molecules, 20 (5) (2015) 8856.

[12] Liu, C.X., Zhang, D.R., He, Y., Zhao, X.S., and Bai, R., Journal of Membrane Science, 346 (1) (2010) 121.

[13] Cruz, M.C., Ruano, G., Wolf, M., Hecker, D., Vidaurre, E.C., Schmittgens, R., and Rajal, V.B., Chemical Engineering Research and Design, 94 (2015) 524.

[14] Furlan, P.Y., Fisher, A.J., Melcer, M.E., Furlan, A.Y., and Warren, J.B., Journal of Chemical Education, 94 (4) (2017) 488.

[15] Sahu, D., Sarkar, N., Sahoo, G., Mohapatra, P., and Swain, S.K., Sensors and Actuators B: Chemical, 246 (2017) 96.

[16] Abou El-Nour, K.M.M., Eftaiha, A., Al-Warthan, A., and Ammar, R.A., Arabian Journal of Chemistry, 3 (3) (2010) 135.

[17] Matej, B., Nina, D., Ludmila, B., Erika, D., Ludmila, T., Jaroslav, B., Maria, V., Miriama, B., Anna, Z., and Peter, B., Advanced Powder Technology, 28 (12) (2017) 3307.

[18] Iravani, S., Korbekandi, H., Mirmohammadi, S.V., and Zolfaghari, B., Research in Pharmaceutical Sciences, 9 (6) (2014) 385.

[19] Xie, P., Ji, W., and Wei, Zh., Characterization and Application of Nanomaterials, 1 (2018) 40.

[20] Alarcon, E.I., Udekwu, K., Skog, M., Pacioni, N.L., Stamplecoskie, K.G., González-Béjar, M., Polisetti, N., Wickham, A., Richter-Dahlfors, A., Griffith, M., and Scaiano, J.C., Biomaterials, 33 (19) (2012) 4947.

[21] Francis, S., Joseph, S., Ebey, P.K., and Beena, M., Journal of Artificial Cells, Nanomedicine, and Biotechnology, 46 (4) (2017) 795.

[22] Verma, Sh., Rao, B.T., Srivastava, A.P., Srivastava, D., Kaul, R., and Singh, B., Colloids and Surfaces A: Physicochemical and Engineering Aspects, 527 (2017) 23.

[23] Iconaru, S.L., Chapon, P., Coustumer, Ph.L., and Predoi, D., The Scientific World Journal, 2014 (2014) 1.

[24] Elsupikhe, R.F., Shameli, K., Ahmad, M.B., Ibrahim, N.A., and Zainudin, N., Nanoscale Research Letters, 10 (2015) 1.

[25] Asghar, M.A., Zahir, E., Shahid, S.M., Khan, M.N., Asghar, M.A., Iqbal, J., and Walker, G., LWT – Food Science and Technology, 90 (2018) 98.

[26] Remya, V.R., Abitha, V.K., Rajput, P.S., Rane, A.V., and Dutta, A., Chemistry International, 3 (2) (2017) 165.

[27] Imam, H., Elsayed, K.A., Ismail, L.Z., Afify, M., and Khedr, M.A., Life Science Journal, 10 (4) (2013) 401.

[28] Pastoriza-Santos, L.M. and Liz-Marzan, L., Nano Letters, 2 (8) (2002) 903.

[29] Abd, A.N., Ismail, R.A., and Habubi, N.F., Journal of Materials Science: Materials in Electronics, 26 (2015) 9853.

[30] Tsuji, M., Hashimoto, M., Nishizawa, Y., Kubokawa, M., and Tsuji, T., Chem. Eur. J., 11 (2) (2005) 440.

[31] Zhang, X.-F., Liu, Z.-G., Shen, W., and Gurunathan, S., International Journal of Molecular Sciences, 17 (9) (2016) 1534.

[32] Wiley, B., Sun, Y., Mayers, B., and Xia, Y., Chem. Eur. J., 11 (2) (2005) 454.

[33] Wiley, B.J., Im, S.H., Li, Z.Y., McLellan, J., Siekkinen, A., and Xia, Y., Journal of Physical Chemistry B, 110 (32) (2006) 15666.

[34] Iravani, S., Korbekandi, H., Mirmohammadi, S.V., and Zolfaghari, B., Research in Pharmaceutical Sciences, 9 (6) (2014) 385.

[35] Tarasenko, N., Butsen, A., Nevar, E., and Savastenko, N., Applied Surface Science, 252 (13) (2006) 4439.

[36] Kawasaki, M. and Nishimura, N., Applied Surface Science, 253 (4) (2006) 2208.

[37] Fazio, E., Gökce, B., De Giacomo, A., Meneghetti, M., Compagnini, G., Tommasini, M., Waag, F., Lucotti, A., Zanchi, C.G., Ossi, P.M., Dell'Aglio, M., D'Urso, L., Condorelli, M., Scardaci, V., Biscaglia, F., Litti, L., Gobbo, M., Gallo, G., Santoro, M., Trusso, S., and Neri, F., Nanomaterials, 10 (2020) 2317.

[38] Kelly, K.F. and Billups, W.E., Accounts of Chemical Research, 46 (1) (2013) 4.

[39] Majeed, M.S., Mahmoud, S.M., Rasheed, R.M., and Rashad, A.A., Baghdad Science Journal, 21 (1) (2024) 217.

[40] Alhamid, M.Z., Hadi, B.S., and Khumaeni, A., AIP Conference Proceedings, 2202 (2020) 020013.

[41] Karnwal, A., Jassim, A.Y., Mohammed, A.A., Al-Tawaha, A.R.M.S., Selvaraj, M., and Malik, T., Frontiers in Microbiology, 16 (2025) 1517772.

[42] Muteeb, G., Rehman, M.T., Shahwan, M., and Aatif, M., Pharmaceuticals, 16 (11) (2023).

[43] Majeed, M.S., Mahmoud, S.M., Rashad, A.A., and Rasheed, R.M., Baghdad Science Journal, 21 (1) (2024) 217.

[44] Koohpeima, F., Mokhtari, M.J., and Khalafi, S., Journal of Applied Oral Science, 25 (4) (2017) 367.

[45] Almashhadani, M.A. and Qassim, W.S., Regulatory Mechanisms in Biosystems, 16 (1) (2025) 1.

[46] Sultan, S.M., Yahya, R.T., Sultan, S.J., and Mohammed, A.A.-H., Medical Journal of Babylon, 22 (1) (2025) 175.

[47] Godakhindi, V., Kravitz, E., and Vivero-Escoto, J.L., Molecules, 30 (3) (2025) 626.

[48] Al-Youzbakee, Z.M. and Mohammad, K.O., Annals of the College of Medicine, Mosul, 46 (2) (2024) 159.

[49] Liu, Q., Liu, C., Wang, S., Zhang, L., Sun, H., and Liao, X., Journal of Hazardous Materials, 489 (2025) 137663.

[50] Kain, H., Gupta, E., Sharma, P., Haldiya, A., Srivastava, V.K., Neeraj, R.R.K., and Kaushik, S., Biofouling, 41 (1) (2025) 1.